CONCRETE LIBRARY OF JSCE NO. 23, JUNE 1994

FE ANALYSIS OF CRACK PROPAGATION IN PLAIN CONCRETE USING SMEARED CRACK MODEL WITH CONCEPTS OF FICTITIOUS CRACK MODEL

(Reprint from Proceeding of JSCE, No.466/V-19, May 1993)

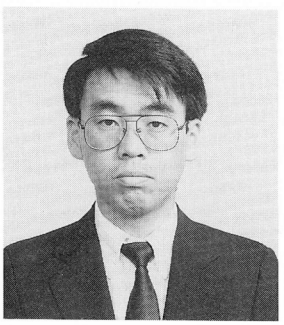

Yuichi UCHIDA

Keitetsu ROKUGO

Wataru KOYANAGI

SYNOPSIS

FE-analysis of cracks in plain concrete specimens was carried out using the smeared crack model and including the concepts of the fictitious crack model. For localized Mode I cracking, the numerical results obtained with this crack model were identical to those with the fictitious crack model. Certain differences of the numerical results between the localized and distributed cracking are demonstrated. The stress locking phenomenon caused by strain softening is also discussed.

Keywords: *smeared crack model, fictitious crack model, FEM, fracture mechanics*

Y. Uchida is an associate professor in the Civil Engineering Department of Gifu University. He received his Doctor of Engineering Degree in 1993 from Kyoto University. His current research interests include the numerical analysis and fracture mechanics of concrete. He is a member of JSCE, JCI and ACI.

K. Rokugo is a professor in the Civil Engineering Department of Gifu University. He received his Doctor of Engineering Degree in 1980 from Kyoto University. His research work covers the failure behavior of concrete and reinforced concrete members. He is a member of JSCE, JCI, ACI, RILEM and CEB.

W. Koyanagi is a professor in the Civil Engineering Department of Gifu University. He graduated and received his Doctor of Engineering Degree from Kyoto University. His research interests cover design methods and the application of new building materials for concrete structures. He is a member of JSCE, JSMS, JCI and ACI.

1. INTRODUCTION

It is well known that there are two basic approaches to crack modeling when analyzing crack propagation in concrete structures with the finite element method(FEM): the discrete crack approach and the smeared crack approach. Since a crack is essentially a surface of discontinuity in displacement, the discrete crack approach is a more direct and intuitive modeling method. However, unless the crack path is known in advance it requires regeneration of the element mesh as the crack propagates. On the other hand, in the smeared crack approach, concrete is treated as a continuum even after cracking, and cracks are modeled as changes in the material properties. Crack propagation can therefore be traced without altering the initial geometric conditions. Consequently, the smeared crack approach is very frequently used, especially in the analysis of reinforced concrete structures.

In this study, the authors attempted analysis of the macroscopic behavior of concrete beams during crack propagation by means of the smeared crack approach, with the focus on unreinforced concrete. Past studies of crack propagation in unreinforced concrete concentrated on beams with notches designed to localize the cracks, and little attention was paid to crack propagation and localization in unnotched beams. Here, the authors investigate how localization of cracking affects the macroscopic behavior of unnotched beams when using the smeared crack approach. They also consider the issue of stress locking, caused by the relationship between crack direction and element mesh, when softening is incorporated into the smeared crack approach.

2. CRACK MODELS BASED ON FRACTURE MECHANICS

The use of fracture mechanics models for the analysis of crack propagation in concrete has recently been attracting attention. Such models are characterized by the application of energy criteria resulting from a consideration of fracture mechanics, i.e., criteria based on softening – instead of conventional strength criteria – which assume that a crack occurs when the stress reaches the tensile strength and the tensile resistance is then completely lost. Adoption of such energy criteria is reported to solve one of the major problems associated with the use of conventional strength criteria, i.e., the dependence of the analytical results on element size [1]. It has also been reported that the so-called "size effect" of strength becomes expressible [2]. Typical fracture mechanics models incorporating energy criteria are the fictitious crack model by Hillerborg et al. [3], which is a discrete crack approach, and the crack band model by Bazant et al. [2], which is a smeared crack approach. Dahlblom et al. [4] proposed another model in which the concepts of the fictitious crack model are applied to the smeared crack approach.

In the fictitious crack model [3], the propagation of a crack is expressed in terms of the separation of nodal points, between which a cohesive force acts. This force is determined from the tension softening curve according to the distance between the nodal points, i.e., the crack width. The tension softening curve is a modeled relationship between crack width and stress transmitted across the crack which is obtained from a uniaxial tension test. The area below the curve is equivalent to the fracture energy, G_F.

In the crack band model [2], the crack is expressed as a continuum with a finite width (crack band width, w_c), whose properties are uniform across the width. Softening is incorporated into the stress-strain relationship ($\sigma - \varepsilon_{cr}$) within the crack band. The strain, ε_{cr}, in this stress-strain relationship is related to the crack band width, w_c, and the crack width, ω, in the tension softening curve ($\sigma - \omega$)

of the fictitious crack model by the expression $\omega = w_c \varepsilon_{cr}$. Also, the area below the stress-strain curve, g_f, is related to the area below the tension softening curve (i.e., the fracture energy, G_F), by the expression $G_F = w_c g_f$. The crack band model is therefore formally equivalent to the fictitious crack model, while having as a characteristic the assumption that the crack band width is a material property.

On the other hand, in applying the fictitious crack model to the smeared approach, Dahlblom et al. [4] assume in their model that the elements containing the crack consist of a fictitious crack and an elastic zone. They determine the stress-strain relationship of an element by combining the properties of the fictitious crack and those of the elastic zone. When combining these properties, the concept of "equivalent length" is introduced in order to incorporate the element size. In other words, a characteristic of this model is that the stress-strain relationship after cracking depends on the element size.

Incidentally, the defect that all these models have in common is that they cannot analyze the microscopic behavior of the concrete near the crack nor the behavior in the fracture process zone. They are only able to consider the macroscopic behavior of a member. In recent years, nonlocal continuum models have been attracting attention as methods which overcome this defect. These models, such as the nonlocal microplane model, treat all material properties as continuous, and ignore macroscopic cracking.

3. ELEMENT PROPERTIES AND METHOD OF ANALYSIS

(1) Material Properties

(a) Outline

In this study, concrete is assumed to be a linear elastic body until a crack occurs. In other words, all nonlinear behavior of a member is attributed solely to cracking. Cracking is assumed to occur when the maximum principal stress exceeds the tensile strength, in a direction normal to the orientation of the maximum principal stress. After cracking, the concrete is assumed to be an orthotropic material, and element properties are determined according to a coordinate system based on the crack direction, as shown in Fig. 1. These properties are then transformed into the global coordinate system using a coordinate transformation matrix. Whereas the stress-strain relation in the direction parallel to the crack remains that of a linear elastic material, tension softening is incorporated into the stress-strain

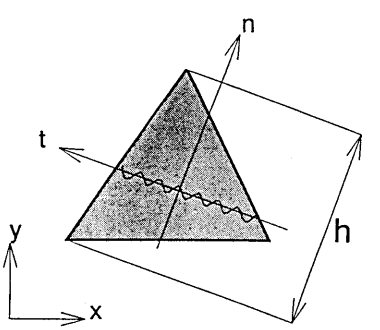

Fig. 1 Local Coordinate and Equivalent Length

relationship normal to the crack. Two models, the fixed crack model and the coaxial rotated crack model, are used for stress evaluations in cases where the direction of the principal strain changes after cracking. In the fixed crack model, the direction of the crack is fixed after cracking, and when the direction of the principal strain changes, shear transfer in the crack plane is considered. This model therefore requires a constitutive model of shear transfer, in addition to the principal strain-versus-principal stress relationship. On the other hand, in the coaxial rotated crack model, the direction of the crack is rotated when the principal strain direction rotates after cracking, making the crack normal to the maximum principal strain. Thus, the direction of the principal strain always coincides with the direction of the principal stress. It is difficult to physically understand what rotation of the crack means, but the consequence of adopting this model is that it requires no material parameters for the analysis of shear properties, since there is no shear stress in the crack plane.

(b) Stress-strain relationship of crack elements

The fictitious crack model yields the behavior of the member after cracking not by considering the stress-strain relationship but by the stress-crack width relationship, or the tension softening curve. It is therefore necessary to convert the crack width to an appropriate strain value when applying this model to the smeared crack approach. For simplicity's sake, a situation is assumed in which a single crack occurs in a one-dimensional element with a length L. Since overall deformation of the element is given as the sum of crack width and elastic deformation of the elastic zone except the crack, the relationship between the average strain of the element and the stress is given by

$$\varepsilon = \frac{\sigma}{E} + \frac{\omega(\sigma)}{L} \tag{1}$$

where $\omega(\sigma)$ is the tension softening curve (σ: stress; ω: crack width), L is the element length, E is the modulus of elasticity, and ε is the average strain in the direction normal to the crack.

In this study, the above equation is adopted as the stress-strain relationship in the direction normal to the crack in the plane elements. However, 3-node constant strain elements are employed here, and as proposed by Dahlblom et al. [3], the length of the element projected in the direction parallel to the crack, h, is adopted as the element size, L, in Eq. (1). This is shown in Fig. 1. This h is hereafter referred to as the "equivalent length" of the element. Where unloading (decrease in strain) occurs after cracking, the origin-oriented curve shown in Fig. 2 is adopted. The 1/4 model shown in Fig. 3 is adopted as the tension softening curve, because it agrees relatively well with normal strength

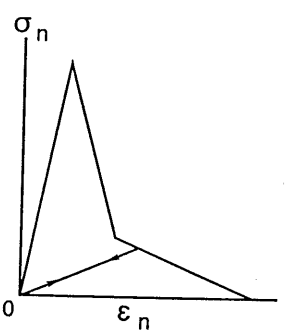

Fig. 2 Tensile Stress - Strain Relation

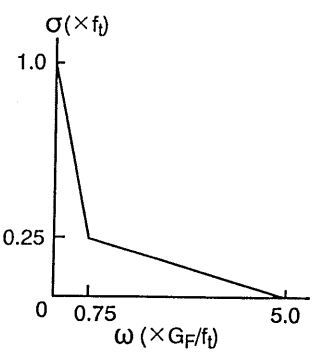

Fig. 3 Tension Softening Diagram

concrete. When such a 1/4 model is used as the tension softening curve, an equivalent length which exceeds the characteristic length of the concrete, $l_{ch}(= EG_F / f_t^2)$ causes the stress-strain relationship in the direction normal to the crack to snap back after the tensile strength is reached. The equivalent length is therefore made smaller than the characteristic length when discretizing the mesh. In the case of the fixed crack model, zero shear stress is assumed on the crack plane as the simplest shear transfer model at the crack. In this model, the shear retention factor is assumed to be zero, as in analysis by means of ordinary orthotropic models.

(2) Solution Procedure and Evaluation of Element Stiffness

In this analysis, an incremental-iterative solution procedure is employed to determine nonlinear solutions. The analysis is carried out under displacement control, thus making possible analysis beyond the point of maximum yield strength. Consequently, problems associated with snapbacks during loading cannot be analyzed. The stiffness matrix is rewritten only at the first convergent iterative computation for each incremental loading step(enforced displacement), and is not rewritten at the second and later iterative computations. This is "modified Newton-Raphson method". The tangent stiffness matrix, however, is not used here.

As explained in the previous section, the constitutive relationship for the material in this analysis is stated not in terms of increments but rather in terms of the total stress- strain relationship. The element stress can therefore be directly computed from the given total strain, instead of by successive integrations of the tangent stiffness. Thus the material stiffness matrix, [D], used for the convergence computation at each loading step should not necessarily be the tangent stiffness of the material's stress-strain relationship, because it is not involved in the stress computation at all but rather is used only to redistribute the unbalanced force. A [D] matrix which yields a steady and efficient convergence should be selected [6]. The authors adopted the [D] matrix described below, which yields steady solutions for all the problems presented in the next section. Fig. 4 shows the flow chart for the computation.

The [D] matrix for a linear elastic body is employed until cracking occurs. The post-crack stiffness in the direction normal to the crack is commonly set near to zero in the analysis of reinforced concrete, but here the value is reduced gradually after the tensile strength is reached, so as to stabilize convergence of the solution (see Eq. (6)). The stiffness in the direction parallel to the crack is allowed to remain elastic. The term expressing Poisson's effect is set at zero.

The shear stiffness is given a value of 1/1000 of the elastic stiffness in the case of the fixed crack model so as to stabilize the solution. On the other hand, the shear stiffness term in the case of the coaxial rotated crack model is introduced only to match the direction of the principal strain with that of the principal stress independently of the material properties. In other words, if the shear stress increases by $\Delta\tau$ from a state of equilibrium after cracking (a state in which the directions of the principal strain and principal stress coincide and the directions of the minimum principal strain and cracking coincide), the change in the direction of the principal stress, $\Delta\theta_s$, is

$$\tan 2\Delta\theta_s = \frac{2\Delta\tau}{\sigma_{nn} - \sigma_{tt}} \tag{2}$$

If the increase in shear strain is $\Delta\gamma$, the change in the direction of the principal strain, $\Delta\theta_e$, is

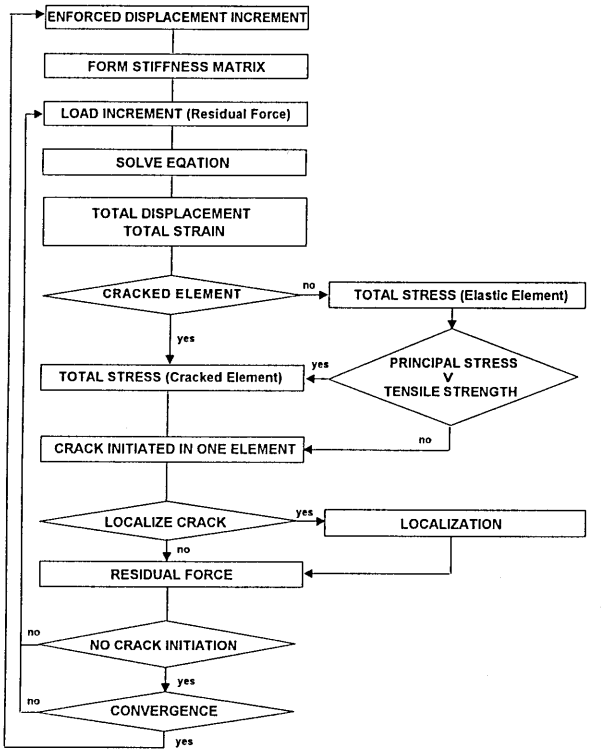

Fig. 4 Flow Chart for Analysis

$$\tan 2\Delta\theta_e = \frac{\Delta\gamma}{\varepsilon_{nn} - \varepsilon_{tt}} \tag{3}$$

Therefore, in order to ensure that the directions of the principal strain and the principal stress always match, G_{nt} should be

$$G_{nt} = \frac{\Delta\tau}{\Delta\gamma} = \frac{\sigma_{nn} - \sigma_{tt}}{2(\varepsilon_{nn} - \varepsilon_{tt})} \tag{4}$$

By integrating all of the above, it follows that :
Before cracking,

$$[D] = \frac{E}{1-\nu^2}\begin{bmatrix} 1 & \nu & 0 \\ 0 & 1 & 0 \\ 0 & 0 & \dfrac{1-\nu}{2} \end{bmatrix} \tag{5}$$

where E is Young's modulus and ν is Poisson's ratio;
and after cracking,

$$\begin{bmatrix} \sigma_{nn} \\ \sigma_{tt} \\ \tau_{nt} \end{bmatrix} = [D_{nt}] \begin{bmatrix} \varepsilon_{nn} \\ \varepsilon_{tt} \\ \gamma_{nt} \end{bmatrix} \tag{6}$$

where σ and ε are stress and strain in the crack coordinate system respectively, n and t in the direction perpendicular and parallel to the crack, and $[D_{nt}]$ is the following:

$$[D_{nt}] = \begin{bmatrix} \mu E & 0 & 0 \\ 0 & E & 0 \\ 0 & 0 & G_{nt} \end{bmatrix} \tag{7}$$

where $\mu = \sigma_n / f_t$ (where σ_n is the stress in the direction perpendicular to the crack in the preceding loading step and f_t is the tensile strength),

$$\begin{aligned} G_{nt} &= G / 1000 && \text{[fixed crack model]} \\ &= \frac{\sigma_{nn} - \sigma_{tt}}{2(\varepsilon_{nn} - \varepsilon_{tt})} && \text{[coaxial rotated crack model]} \end{aligned} \tag{8}$$

where $G\ (= E / 2(1+\nu))$ is the shear elastic modulus.

The convergence of solutions is judged as follows:

$$\frac{\sum (\Delta f_i)^2}{\sum (f_i)^2} \leq 1.0 \times 10^{-6} \tag{9}$$

where f_i is the external nodal force and Δf_i is the unbalanced equivalent nodal force.

4. ANALYTICAL RESULTS AND DISCUSSION

(1) Analysis under Mode I Loading

Unreinforced concrete beams under flexure with a cross-section of 10×10cm and a loading span of 30cm were analyzed. The tensile strength of the concrete was assumed to be 30kgf/cm^2, the fracture energy to be 0.1kgf/cm, and the modulus of elasticity to be 3.0×10^5kgf/cm^2, thus simulating a concrete of normal strength. The 1/4 model was adopted for the tension softening curve. The analysis was premised on plane stress conditions throughout.

(a) Discrete crack approach and smeared crack approach

Firstly, analysis was carried out with the element mesh simulating third-point loading, as shown in Fig. 5, using both the discrete crack approach (fictitious crack model) and the smeared crack approach for comparison. Making use of the arrangement's symmetry, only one half of the beam was analyzed. In the analysis by the discrete crack approach, one single crack was assumed to occur at the center of the tension edge and propagate vertically upward. Since details are available in

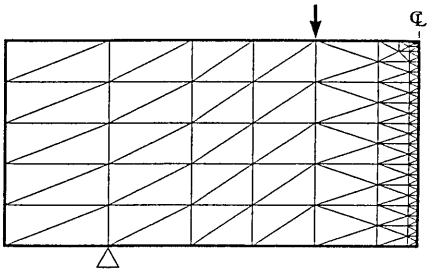

Fig.5 Discretization of Model for Analysis by Discrete and Smeared Crack

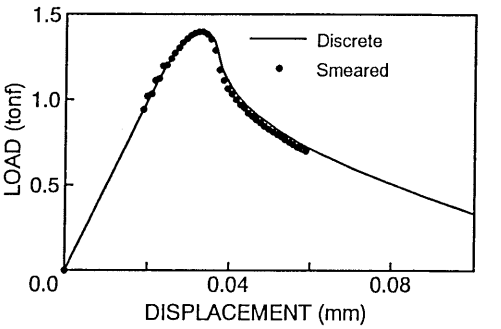

Fig.6 Analytical Results of Discrete and Smeared Crack Models

reference [7], the computational method for this approach is not described here. In analysis by the smeared crack approach, the crack was assumed to occur only in a vertical row of elements along the symmetry line, in order to localize the crack at the central cross-section of the beam. That is, the conditions match those of the discrete crack approach.

Fig. 6 shows the load-displacement curves obtained from this analysis. It was confirmed that the results obtained by the two approaches coincide exactly. It should be noted that when using the smeared crack approach, the equivalent length of the interface crack elements has to be twice the value calculated as the length projected in the direction of the crack, because only one half of the specimen is modeled and the symmetry line coincides with the crack path. Otherwise twice the prescribed fracture energy would be dissipated in the analysis process. Similarly, when using the discrete crack approach, the crack width has to be made twice the displacement of the cracked node point, and the cohesive force across the crack determined from this crack width has to be applied as the equivalent nodal force. In other words, if a crack propagates along the symmetry line of a beam which is only partly modeled, it has to be treated differently from cracks in other locations.

(b) Dependence on element size

Analysis was carried out for three mesh sizes under center-point loading, as shown in Fig. 7, to investigate the effects of element size on the results. Here again the crack was assumed to occur only along the vertical row of elements in the center of the beam. The results are plotted in Fig. 8. Though the initial stiffness was higher in (a) with large elements, the overall shape and maximum yield strength in all three cases nearly coincided. This verifies that the use of models which take account of equivalent length eliminates the element size dependence. The high initial stiffness of (a) may be attributed to the low accuracy of the analysis in the elastic zone due to the large mesh.

(c) Localization of cracking

In the case of the above smeared crack approach, it is assumed that no cracking takes place in elements other than the row at the center of the beam. The maximum load on the beam, however, is nearly 1.4 times higher than the load at which the stress on the tension edge reaches the tensile strength, because tension softening is taken into account. It follows that there are elements a side from those in the center in which the stress is higher than the tensile strength. Therefore, a further smeared crack analysis was conducted by applying only the principal stress criteria for the judgment of the onset of cracking, without assuming the crack path in advance and without consideration of crack localization. In this analysis the entire beam was modeled, as shown in Fig. 9, for the reason

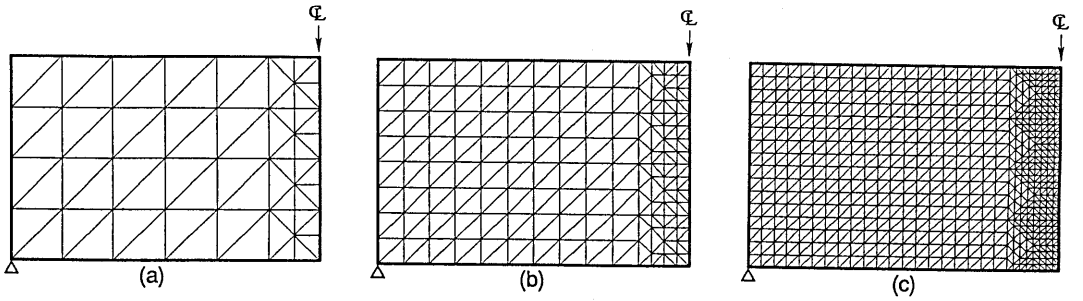

Fig.7 Discretization of Model for Analysis of Dependency of Mesh Size

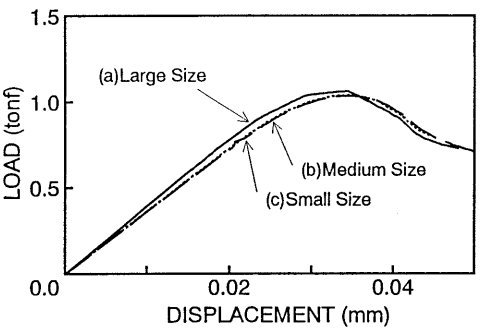

Fig.8 Influence of Mesh Size

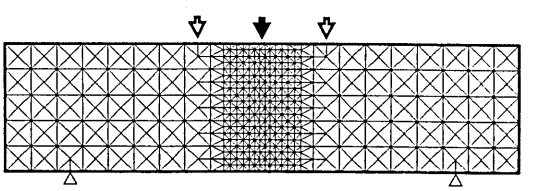

Fig.9 Discretization of Model for Analysis of Influence of Localization

mentioned above. Both third-point loading and three-point loading were analyzed.

Fig. 10 shows the results of this analysis in the case of third-point loading. The results for the case where the crack was assumed to be localized to the mid span elements is also included in the figure. In the case of distributed cracking, the enforced displacement was controlled such that it increased in one step up to the point immediately before cracking, and then in increments of 1/2000 mm. If the solution began to diverge or oscillate, the increment was reduced further, and iterative computations were continued until the convergent conditions shown in Eq. (9) were fulfilled. After the onset of cracking, 70 steps were required before the maximum load was reached. In the case of localized cracking, the increment in displacement was 1/1000 mm after the onset of cracking. Twelve steps were required until the maximum load was reached. Fig. 10 reveals that the maximum load as well as the displacement at the maximum load were higher in the case of distributed cracking than in the case of localized cracking.

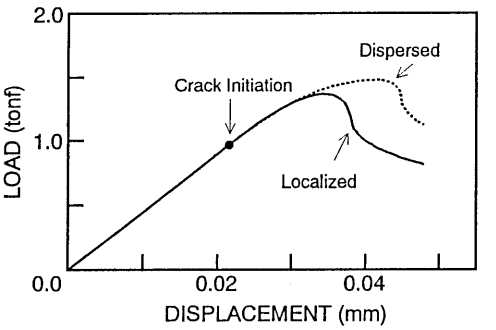

Fig.10 Load-Displacement Curves under Third-Point Loading

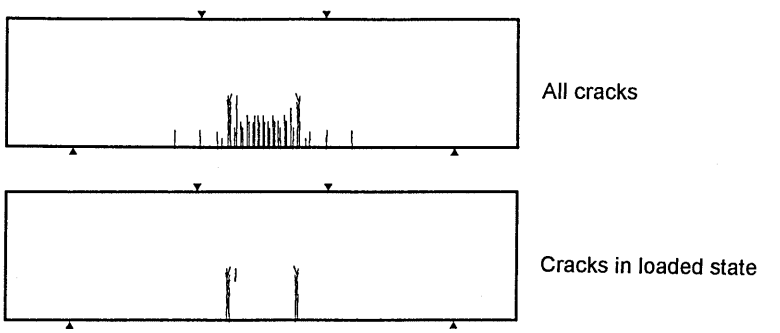

Fig.11 Crack Pattern (Third-Point Loading)

Fig. 11 shows the cracking pattern at the point of maximum load in the case of distributed cracking. While Fig. 11(a) shows all cracks that had occurred by that time, Fig. 11(b) shows only those cracks which occurred in the loaded elements; that is, the elements in which the stress-strain relation is on the envelope of the stress-strain curve shown in Fig. 2. These figures reveal that, in the case of distributed cracking, the cracks occur over the entire tension edge within the moment span. By the time of maximum load, many of these cracks have reached the unloaded state, while the cracks in the loaded state are divided into two lines, instead of concentrating in one.

The reason for the high load in the case of dispersed cracking can be explained. Suppose a uniform bar is under uniaxial tension, as shown in Fig. 12, for the sake of simplicity. If cracking is distributed, the shape of the softening region in the entire bar's load-displacement curve, – i.e., the average stress-strain curve – depends on the number of cracks occurring in the member. The slope of the curve becomes gentler as the number increases. Similarly, when more than one crack occurs on the tension side of a beam specimen, the slope of the softening region of the average stress-strain curve on the tension edge becomes gentler. This leads to the increase in beam, just as the flexural strength increases as the slope of the tension-softening curve becomes gentler in the discrete crack approach.

The analytical results for the three-point loading with localized and distributed cracking are shown in Fig. 13. Fig. 14 shows the cracking at the time of the maximum load. The coaxial rotating model was used in this analysis, and the displacement increments were the same as in the case of third-point

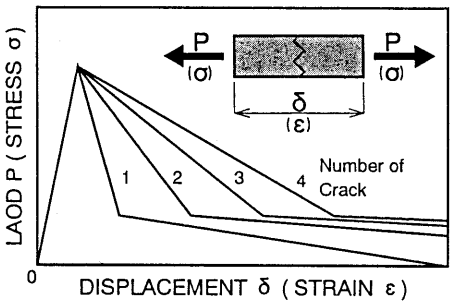

Fig.12 Load-Displacement (Stress-Strain) Relations of One Element

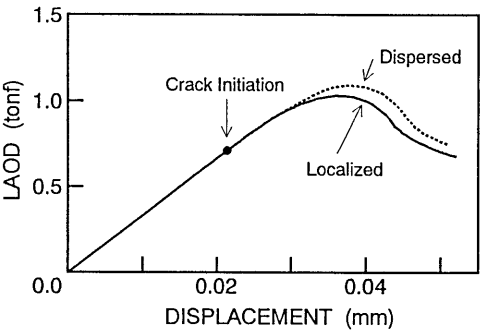

Fig.13 Load - Displacement Curves under Three-Point Loading

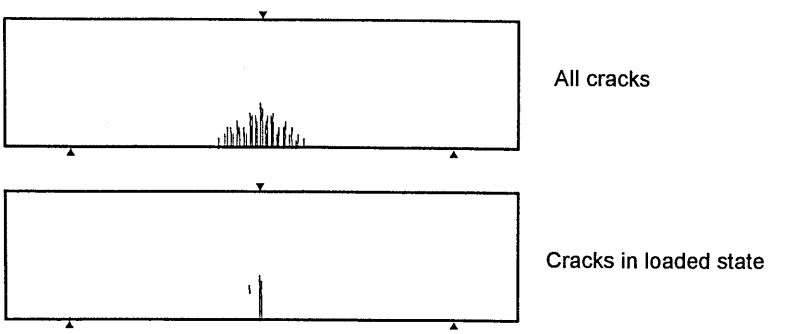

Fig.14 Crack Pattern (Three-Point Loading)

loading. Since the flexural moment is a maximum at the central cross-section of the specimen in the case of three-point loading, cracking naturally tends to congregate in the center of the specimen even without intentional localization. The difference between the load-displacement curves for localized and distributed cracks is less than in the case of third-point loading.

As a result of the above, it is considered that an operation to localize cracking to a row of elements is necessary when using the smeared crack approach adopted in this study to analyze a member, such as an unreinforced concrete beam under third-point loading; that is, in a member in which the cracking occurs in a region where the stress conditions are uniform immediately before cracking and in which it is localized as it propagates. It is also necessary to introduce a parameter to determine the range of influence of localization in the direction normal to the crack, i.e., a localization limiter. Here, the method of crack localization adopted is that as cracking develops, if the centroids of neighboring elements falls within the projection area in the direction normal to cracking in the crack-tip element, they are assumed to be noncracking elements. This is shown in Fig. 15. The element adjacent to the crack-tip element and ahead of the crack is assumed to remain a crackable element. By adopting this method, the cracking of a flexural beam can be localized to a single row of elements without assuming a particular crack path in advance, and the analytical results are the same as those obtained when a crack path is assumed in advance. Though cracking may be localized in this manner, probability theory has to be introduced to specify the first element which cracks within the region of uniform stress. Here, this first crack element was assumed to be the lowermost element in the center of the beams, for the sake of simplicity. The localization limiter determining the range of influence of

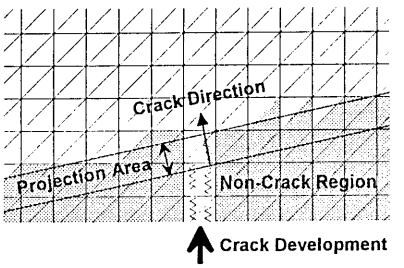

Fig.15 Procedure of Crack Localization

localization was assumed to be significantly larger than the beam. In other words, only one crack was assumed to occur in a beam. This is a prerequisite to the discrete crack approach as well, and corresponds to the discrete cracks interval [8]. In a case where the stress is non-uniform from the beginning, such as under three-point loading, the results for distributed cracking may be close to those for localized cracking. In this study, rather small displacement increments were adopted, but the influence of increment size on the results was not investigated. This is a issue to be investigated in the future.

(2) Crack Propagation Analysis under Mixed-mode Loading

Although the terms Mode I (tension) and Mode II (in-plane shear) are not used for reinforced concrete members, the so-called shear fracture – fracturing under shear loading – is still being actively studied. As regards analysis, a number of studies have focused on this as a problem of shear transfer across a crack plane, and a variety of models have been proposed. Most of them, however, model a visible crack wider than 0.1 mm, across which reinforcement is arranged or a confining force acts in the direction normal to the crack. Thus they model the so-called interlocking effect of the aggregates.

On the other hand, in the case of unreinforced concrete members, no answer has yet been obtained to even such simple question as whether fracture in Mode II is practically possible or not. There is nor any experimental data on shear properties within a fracture process zone or on the state of microcracking immediately after tension softening. The crack width of normal concrete is as small as 0.025 mm at the knee point of the tension softening curve used in this study, i.e., the point where the stress decreases to a quarter of the tensile strength. It would be extremely difficult to conduct shear tests while controlling such a small crack width. Analytically, Rots [9] and Bocca et al. [10] reported on the analysis of unreinforced concrete beams under mixed-mode loading. According to their reports, however, most experimental results for unreinforced concrete under mixed-mode loading can be simulated by an analysis which considers only Mode I fracture.
Here the applicability of this method of analysis to unreinforced concrete beams under mixed-mode loading is discussed as well as a problem associated with such an application. In the analyses, the crack onset conditions, direction of crack occurrence, and element properties were assumed to be the same as the Mode I cracking, and the Mode II fracture conditions were not included, in consideration of the results by Rots and Bocca et al.

(a) Outline of experiments

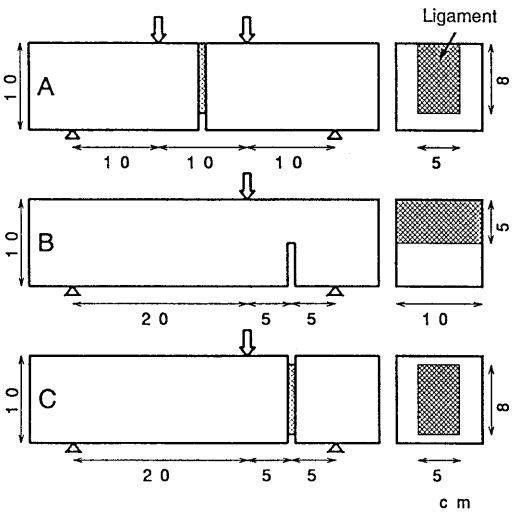

Fig.16 Dimensions of Specimens

Three types of notched specimen as shown in Fig. 16 were used in the experiments. A test method with simple boundary conditions and easy loading was selected here, out of such mixed mode test using the double notched shear beam which is loaded anti-symmetrically or using push-off specimens. Specimen A is a Mode I specimen with a notch 4.5mm wide extending over the bottom edge and both sides. Specimens B and C were subjected to mixed-mode loading. Specimen B has a notch only on the bottom edge, from which skew crack development can be expected. Specimen C has a notch around the entire perimeter of the fracture cross-section designed to maximize the influence of Mode II loading by predetermining the crack path. The load and displacement at the loading point were measured during the loading tests. The concrete was a normal strength concrete with a maximum aggregate size of 15mm. The compressive strength(ϕ10×20cm), splitting tensile strength (ϕ15×20 cm), and modulus of elasticity were 317kgf/cm^2, 28.5kgf/cm^2, and 3.3×10^5kgf/cm^2, respectively. Four to six specimens of each type were prepared.

(b) Results of experiments and analyses

Figs. 17 (a) and 18 show the element mesh and the load-displacement curve for Specimen A. The shaded area in Fig. 18 represents the scatter in experimental values. In the analysis, the fracture energy was assumed to be 0.1kgf/cm. The 1/4 model was adopted as the tension softening curve, and plane stress conditions were assumed. Only Mode I cracking occurred in this type of beam, and there was no difference between the results of the fixed crack model and the co-axial rotated crack model. Only the analytical results for the co-axial rotated crack case are shown here. Fig. 18 shows that the experimental and analytical results agree well, thus verifying the adequacy of the fracture energy value assumed in the analysis and the concrete tension softening curve model used in the experiment. The same fracture energy and tension softening curve were thus employed for the analysis of Specimens B and C as described below. Since Specimen A had a notch around the sides as well and the ligament consisted of a single row of elements, the crack occurred only in a single row of elements in the analysis even without an operation to localize the crack.

Fig. 17 (b) shows the element mesh of Specimen B. Fig. 19 shows the results of analysis using the fixed crack model and the co-axial rotated crack model with distributed cracking. Although the peak load and the displacement at peak load is larger in the analyses than in the experiment, the overall

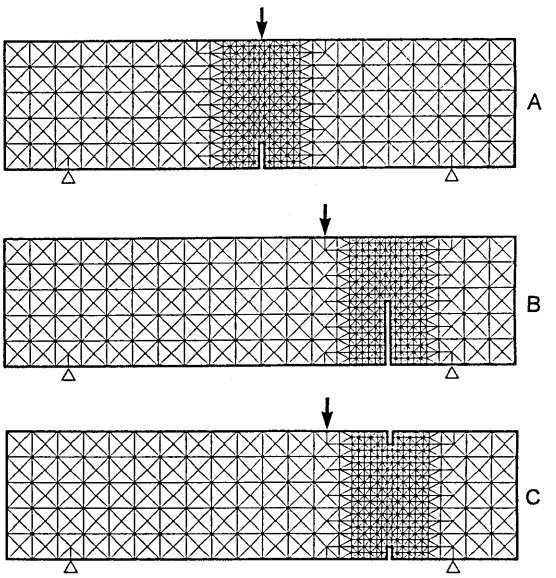

Fig.17 Discretization of Model under Mixed Mode Loading

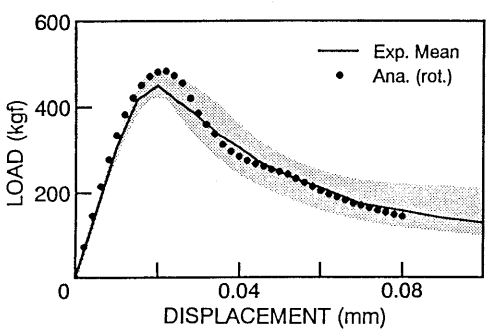

Fig.18 Load-Displacement Curve of Specimen A

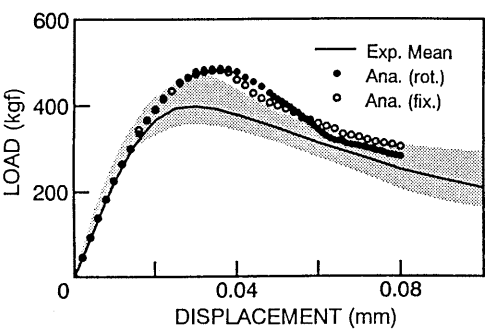

Fig.19 Load-Displacement Curve of Specimen B

shape of the analytical and experimental load-displacement curves practically coincide. Specimen B exhibited little difference between analysis with different crack models, demonstrating that the effects of Mode I cracking overwhelm those of Mode II cracking.

Fig. 20 shows the analytical results for Specimen B using the coaxial rotated crack model with localized cracking ("Mesh a" in the figure). The strength calculated by this analysis was much higher than the experimental value. This may be due to the stress locking phenomenon pointed out by Rots [10]. Fig. 21 shows the distribution of principal tensile stresses, demonstrating that crack localization led to a significant disturbance of the stress conditions around the cracking elements. This can be explained as follows: As shown in Fig. 22, when strain softening is incorporated into the smeared crack approach, softening of a cracking element satisfies the equilibrium and compatibility conditions by unloading in the noncracking elements adjacent to it, if the boundaries between them are parallel to the cracks. If the boundaries are not parallel to the crack, softening of a cracking element – that is, an increase in the principal strain in the direction normal to the cracking – increases the shear strain

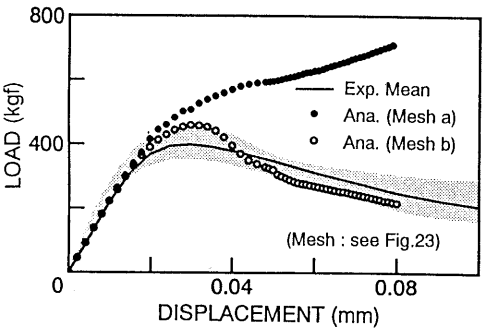

Fig.20 Load-Displacement Curve of Specimen B (Crack Localization)

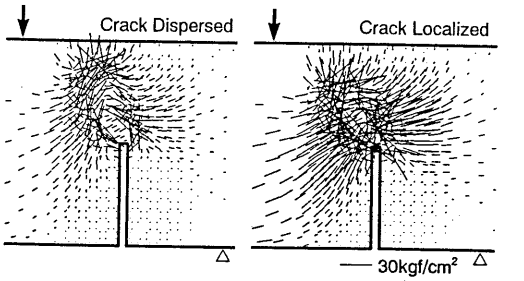

Fig.21 Distribution of Tensile Principal Stress

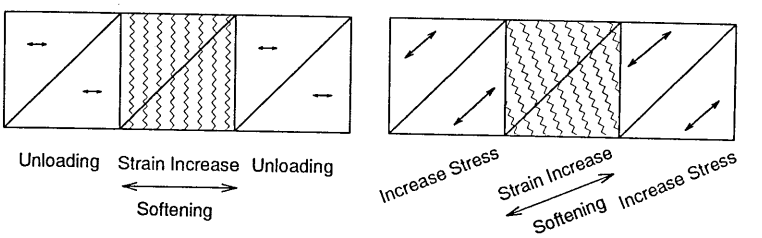

Fig. 22 Stress Locking caused by Compatibility of deformation

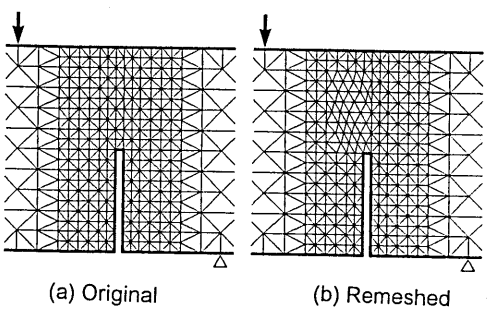

Fig.23 Remeshing of Model

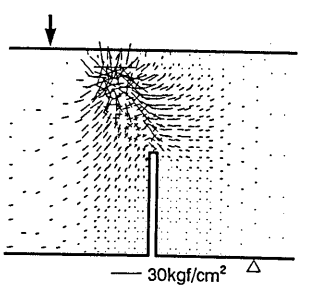

Fig.24 Distribution of Tensile Principal Stress after Remeshing

in the adjacent elements due to the restraint imposed by the compatibility condition. This increases the principal stress, offsetting the decrease in normal stress in nearby elements. In other words, when a cracking element is about to soften, the stress in the adjacent elements increases. This causes a phenomenon known as locking, which hampers the deformation, or softening, of the cracking element, and results in an increase in the strength of the beam.

Though locking inevitably becomes a problem when strain softening is incorporated into the smeared crack approach, its effects may be reduced if the element mesh is so arranged that the direction of the mesh is as parallel as possible to the cracks. Thus an analysis was performed with a mesh pattern which was modified in the region where the dispersed cracking is considered to propagate, as shown in Fig. 23. This yielded a marked improvement regarding locking, as shown in Fig. 24. The load-displacement curve, as shown in Fig. 20 ("Mesh b"), also moved closer to the experiment values than

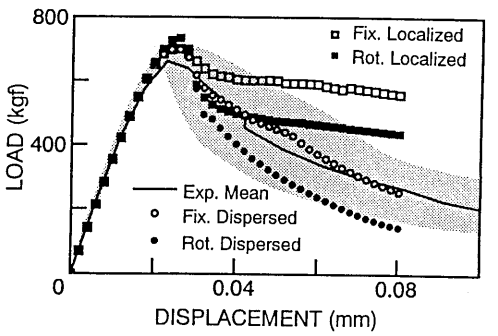

Fig.25 Load-Displacement Curve of Specimen C

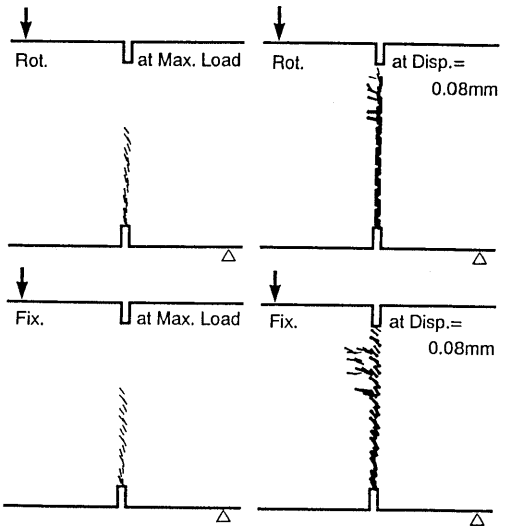

Fig.26 Crack Pattern of Specimen C

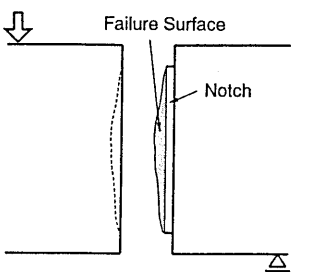

Fig.27 Failure Mode of Specimen C

in the case of analysis of dispersed cracking shown in Fig. 19. This suggests that regeneration of the mesh according to the direction of crack propagation may be an effective way of avoiding the influence of locking.

The load-displacement curves of Specimen C are shown in Fig. 25. Though there is no difference between the curves up to the peak load, the fixed crack model indicates higher loads than those of the coaxial rotated model in the descending region. The curves generated by the analysis with distributed cracking both fall within the range of experimental scatter, though there are some differences between them.

On the other hand, the curves resulting from analysis with localized cracking indicate high loads in the descending region, and they are outside the range of experimental scatter. This is because, as shown in Fig. 26, the cracks tend to escape from the notched section toward the loaded side, leading to intense locking. In the experiments as well, the rupture surface was convex towards the loading side, as shown in Fig. 27. A more accurate investigation of this type of specimen is thought to require three-dimensional analysis.

5. CONCLUSIONS

Various types of analysis were carried out using a model in which the concepts of the fictitious crack model are applied to the smeared crack approach. This model is designed for the FE analysis of the macroscopic fracture phenomenon resulting from crack propagation in unreinforced beams. Analysis confirmed the following characteristics of fracture under Mode I loading:

(1) The results of analysis when the fictitious crack model is applied to the smeared crack approach coincide with the results of the analysis when the fictitious crack model is directly applied to the discrete crack approach.
(2) When applying the concept of the fictitious crack model to the smeared crack approach, the dependence of the analytical results on element size can be eliminated by introducing an equivalent length.

The following new findings were also made:
(1) Analysis of cracks distributed among more than one row of elements and that with cracking localized to a single row of elements leads to different results. A method of localizing the cracking during analysis was proposed.
(2) The load-displacement relationship of specimens under mixed-mode loading as employed in this study can be approximately estimated by the use of a model in which the concept of the fictitious crack model is applied to the smeared crack approach. Care should be exercised, however, to avoid locking during the analysis.
(3) Though the problem of locking is inevitable when strain softening is incorporated into the smeared crack approach, its effects can be reduced to a certain extent by arranging the element mesh parallel to the direction of crack propagation.

Finally, the smeared crack approach used in this study might be dependent on the element mesh, especially in the direction of the element boundaries, as described above. For this reason, care should be exercised when using this approach. This dependence on the element mesh adopted in the analytical method , including the one used in this study, requires more detailed investigation.

References

[1] Rots, J.G., Nauta, P., Kusters, G.M.A. and Blaauwendraad, J.: Smeared Crack Approach and Fracture Localization in Concrete, HERON, Vol. 30, No.1, p.48, 1985.
[2] Bazant, Z.P and Oh, B.H.: Crack Band Theory for Fracture of Concrete, Materials and Structures, Vol.16, No.13, pp.155-177, 1983.
[3] Hillerborg, A., Modeer, M. and Petersson, P.E.: Analysis of Crack Formation and Crack Growth in Concrete by Means of Fracture Mechanics and Finite Elements, Cement and Concrete Research, Vol.6, pp.773-782, 1976.
[4] Dahlblom, O. and Ottosen, N.S.: Smeared Crack Analysis Using Generalized Fictitious Crack Model, Journal of Engineering Mechanics, ASCE, Vol.116, No.1, pp.55-76, 1990.
[5] Bazant, Z.P and Ozbolt, J.: Nonlocal Microplane Model for Fracture, Damage and Size Effect in Structures, Journal of Engineering Mechanics, ASCE, Vol.116, No.11, pp.2485-2505, 1990.
[6] Maekawa, K.: Characteristics of Numerical Calculation in the Nonlinear Analysis of Reinforced Concrete by Means of Finite Element Method, Guide Line for the Application of FEM Analysis to the Design of Concrete Structures, JCI, pp.127-134, 1989 (in Japanese).
[7] Technical Committee on Fracture Mechanics of Concrete, JCI Colloquium on Fracture

Mechanics of Concrete Structures, Part I, Committee Report, JCI, JCI-C19, p.176, 1990.
[8] Bazant, Z.P.: Mechanics of Distributed Cracking, Applied Mechanics Reviews, ASME, Vol.39, No.5, pp.675-705, 1986.
[9] Rots, J.G.: Computational Modeling of Concrete Fracture, Ph.D. Thesis, Delft University of Technology, 1988.
[10] Bocca, P., Carpinteri, A. and Valente, S.: Mixed Mode Fracture of Concrete, International Journal of Solids and Structures, Vol.27, No.9, pp.1139-1153, 1991.